ORNL/SPR-2025/4195

Light Water Reactor Sustainability Program

Complete the Microstructural Characterization on Alloy 182 Samples Produced in FY24 Weld Campaign and Demonstrate the Weldability of Irradiated Ni Alloy 182 (up to 20 appm)

M3LW-25OR0406013

September 2025
U.S. Department of Energy
Office of Nuclear Energy

ORNL/SPR-2025/4195

Materials Science and Technology Division

COMPLETE THE MICROSTRUCTURAL CHARACTERIZATION ON ALLOY 182 SAMPLES PRODUCED IN FY24 WELD CAMPAIGN AND DEMONSTRATE THE WELDABILITY OF IRRADIATED NI ALLOY 182 (UP TO 20 APPM)

M3LW-25OR0406013

Jian Chen, Roger Miller, Zhili Feng
Oak Ridge National Laboratory

Jonathan Tatman, Benjamin Sutton, Gregory Frederick
Electric Power Research Institute

September 2025

Prepared by

OAK RIDGE NATIONAL LABORATORY
Oak Ridge, TN 37831-6283
managed by
UT-BATTELLE, LLC
for the
US DEPARTMENT OF ENERGY
Office of Nuclear Energy
under contract DE-AC05-00OR22725

CONTENTS

LIST OF FIGURES

LIST OF TABLES

ACRONYMS

ABSI-LW	auxiliary beam stress improved laser welding
appm	atom parts per million
DOE	Department of Energy
EPRI	Electric Power Research Institute
HAZ	heat-affected zone
HeIC	helium induced cracking
LTO	Long-Term Operation
LW	laser weld
LWRS	Light Water Reactor Sustainability
NE	Office of Nuclear Energy
ORNL	Oak Ridge National Laboratory
wppm	weight parts per million
Grain boundary degradation	GBD

ACKNOWLEDGMENT

This research was sponsored by the US Department of Energy (DOE), Office of Nuclear Energy (NE), under contract No. DE-AC05-00OR22725 with Oak Ridge National Laboratory (ORNL), managed and operated by UT-Battelle, LLC. Programmatic support was provided by DOE Office of Nuclear Energy (DOE-NE), Light Water Reactor Sustainability Program Materials Research Pathway.

The authors gratefully acknowledge the program support of Xiang (Frank) Chen, Materials Research Pathway Lead of the Light Water Reactor Sustainability Program at ORNL; engineering support of Kurt Smith and Bob Sitterson; hot cell facilities and operations contributions of Clay Morris, Jerid Metcalf, Tony Davis, Kevin Delabar, Rick Bowman, Scott Thurman, Scott White, Donald Caverly, and Allen Smith.

ABSTRACT

This report summarizes the microstructural characterization of irradiated Ni-base alloy 182 laser-welded samples produced at the Radiochemical Engineering Development Center (REDC) in FY24. Irradiated nickel alloy 182 with estimated helium concentration up to 20 appm were laser welded in the hot cell with refined welding parameters. Equipment and capabilities were developed jointly by the U.S. Department of Energy, Office of Nuclear Energy, Light Water Reactor Sustainability Program, the Electric Power Research Institute, the Welding and Repair Technology Center, and Oak Ridge National Laboratory. The significant, on-going effort to weld irradiated alloys with high helium concentrations and comprehensively analyze the results will eventually yield validated repair techniques and guidelines for use by the nuclear industry in extending the operational lifetimes of nuclear power plants.

This report fulfills the FY 2025 milestone M3LW-25OR0406013, “Complete the microstructural characterization on alloy 182 samples produced in FY24 weld campaign and demonstrate the weldability of irradiated Ni alloy 182 (up to 20 appm)”.

1. INTRODUCTION

Today, welding is widely used for repair, maintenance, and upgrades of nuclear reactor components. As a critical technology to extend the service life of nuclear power plants beyond 60 years, weld technology must be further developed to meet new challenges associated with the aging of the plants, such as control and mitigation of the detrimental effects of weld residual stresses and repair of highly irradiated materials. To meet this goal, a fundamental understanding of welding effects is necessary for the development of new and improved welding technologies.

Welding repair of irradiated nuclear reactor materials (such as austenitic stainless steels used for the reactor internals) is very challenging because the existence of helium in the steel, even at very low levels (*i.e.,* parts per million), can cause cracking during repair welding. Helium is a product of the boron and nickel transmutation process under intense neutron irradiation. Under the influence of high temperatures and high tensile stresses during welding, rapid formation and growth of helium bubbles can occur at grain boundaries, resulting in intergranular cracking in the heat-affected zone (HAZ) – the so-called helium-induced cracking (HeIC) (Kanne Jr. 1988). Over the past decades, a basic understanding has been established for the detrimental effects of weld stresses on HeIC (Feng and Wilkowski 2002) (Feng, Wolfe, *et al*. 2009). However, practical methods for weld repair of irradiated materials are still evolving. Industry's experience is based on current arc-welding–based and laser-welding–based repair technologies that are limited to situations where the helium in the irradiated materials is less than 10 appm. Although no welding restrictions are required for helium levels below 0.1 appm helium, restrictions on welding parameters, such as welding heat input, are necessary when the helium levels are above 0.1appm. Reactor internals with helium levels above 5-10 appm are generally considered not to be weldable (or weld repairable) using today's welding practices common to the industry (EPRI 2015) (JNES 2004).

As the service life of nuclear reactors in the United States is extended, the amount of helium in the structural materials in certain highly irradiated areas will continue to increase, reaching levels much higher than 10 appm. Therefore, innovations in repair welding technology are essential to addressing this critical industry need.

This research, a joint effort of the US Department of Energy Office of Nuclear Energy (DOE-NE) Light Water Reactor Sustainability (LWRS) Program and the Electric Power Research Institute (EPRI) Welding and Repair Technology Center, is aimed at developing advanced welding technology for reactor repair and upgrades. It focuses on welding repair of irradiated materials that are extremely challenging and require long-term R&D. Multiple weld campaigns have been completed on irradiated 304 and 316 stainless steels with the targeted helium concentration up to 30 appm between FY2018 and FY2021. Microstructural characterizations demonstrated the feasibility to use advanced auxiliary beam stress improved laser welding (ABSI-LW) to mitigate the formation of HeIC. In FY2022 and FY2023, irradiated nickel alloy 182 samples were further studied using ABSI-LW (M3LW-22OR0406013, M3LW-23OR0406015). The microstructural characterization showed no major cracks in most of the HAZ in welded samples with dopped boron concentration up to 15 wppm, except for weld toe regions as shown in **Figure 1**. Hence, the research activities in FY2024 focused on further optimization of the laser welding parameters to mitigate this issue (M2LW-24OR0406013). This milestone report summarizes the microstructural characterization of the laser welded samples produced in FY24.

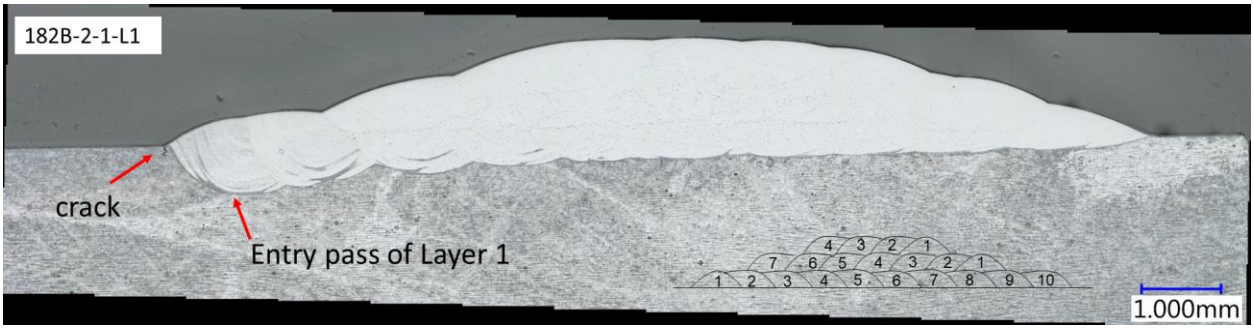

Figure 1 A weld cross-section produced in the previous weld campaign (M3LW-23OR0406015) showing a small crack in the toe region of the entry pass.

2. EXPERIMENTS

2.1 Materials

Five heats of Alloy 182 having five boron concentration levels (nominally 0, 5, 10, 20, and 30 ppm by weight) were produced by Sophisticated Alloys, Inc, following the specifications established by ORNL to cover the anticipated range of helium levels in materials exposed up to 80 years of reactor operation (M3LW-14OR0406014, 2014). **Table 1** shows the complete chemistry analysis of the Alloys 182 heats used in this project. As shown in the **Table 1** not all the target boron concentrations were achieved but a wide range of boron levels were produced ranging from 0.3 to 23 wppm. All other elements met the chemistry requirements for Alloy 182. Bar stock sections were machined to final dimensions (76x56x8.9mm^3 nominal) to yield 7 pieces at each boron level for subsequent irradiation. Alloy 182 is a commonly used nickel-based weld metal for joining Alloy 600 components, particularly in nuclear reactor pressure boundary applications such as nozzles and safe ends. Although most plants are transitioning from Alloy 600 to Alloy 690, using Alloy 152 as the preferred filler metal, due to the superior stress corrosion cracking resistance of Alloy 690, many existing components with Alloy 182 welds remain in service. Additionally, repair welds and overlays often interact with these legacy welds. As such, understanding the behavior of Alloy 182 remains critical for supporting long-term operation and life extension strategies. An additional fifteen specimens from heats 182D and 182E were fusion welded on one side to half of the specimen depth to produce a representative weld microstructure.

The custom alloy 182 blocks were irradiated at the ORNL High Flux Isotope Reactor with a total fluence ranging from 5.08×10^{20} to 1.31×10^{21} n/cm^2, which includes contributions from both fast and thermal neutrons (thermal neutrons < 0.5 eV, epithermal neutrons 0.5 eV to 0.1 MeV and fast neutrons > 1 MeV) depending on the location of the blocks inside the irradiation bores. The irradiated blocks were aged for more than 2 years to allow decay of short half-life isotopes before welding experiments began. Details of the irradiation of the coupons can be found in the previous milestone report M3LW-17OR0406013 (Feng, Miller, *et al*. 2017).

Table 1 Chemistry Analysis Results of Alloy 182

Element	Unit	Alloy 182 Heat Identification				
		182A	182B	182C	182D	182E
B	wppm	0.3	5	15	14	23
Co	wppm	2	2	2	2	2
Al	wppm	81	34	32	54	56
Mo	wppm	1	1	8	1	1
Cu	wppm	2	1	2	1	1
C	wt%	0.03	0.08	0.03	0.04	0.04
Mn	wt%	7.03	7.00	6.76	7.17	7.08
Si	wt%	0.50	0.50	0.51	0.50	0.49
Cr	wt%	15.99	16.00	16.00	16.16	16.10
Fe	wt%	7.36	7.92	7.31	7.14	7.12
Nb	wt%	2.07	2.06	1.83	1.82	1.84
Ti	wt%	0.44	0.43	0.43	0.43	0.46
P	wt%	0.00013	0.00011	0.00018	0.00015	0.00016
S	wt%	0.00207	0.00199	0.00280	0.00200	0.00220
Ni		Balance	Balance	Balance	Balance	Balance

2.2 Welding

In this weld campaign, laser welding experiments were conducted on three alloy 182 coupons with three nominal boron concentrations (10, 20 and 30 wppm). The weld coupon ID, measured boron concentrations, welding process, and weld campaign identification are given in **Table 2.** Details of the equipment and experimental procedures have been reported in the previous milestone report (M3LW-23OR0406015) (Chen, *et al*. 2023).

Table 2 Weld Coupon ID

Weld Coupon ID.	Microstructural condition	Target Boron, wppm	Measured boron, wppm
182C-4	Wrought	10	15
182D-3	Wrought	20	14
182E-1	Wrought	30	23

Laser weld cladding was performed on irradiated alloy 182 base material with 52M as filler material. Four laser-welded clads (weld IDs L1, L2, L3 and L4) were made using different welding conditions on each coupon. The arrangement of the four laser clads on each coupon was identical to the previous weld campaign (M3LW-22OR0406013). Two claddings on the top side of the steel coupon plate are labeled as L1 and L2 welded using relatively low heat input, and another two on the bottom side are labeled as L3 and L4 welded using high heat input. Weld claddings L2 and L4 in the figure were made with the ABSI-LW and weld claddings L1 and L3 were made with LW without ABSI for comparison. The selection of different heat input levels was aimed at generating data points for identifying the threshold heat input above which HeIC occurs, as a function of helium concentration. The application of ABSI can reduce tensile stresses during weld solidification, thereby decreasing the susceptibility to HeIC.

Each clad consisted of three layers (Layer 1, layer 2 and Layer 3 from the bottom to the top of each clad). Layer 1 consisted of ten weld passes. Layer 2 consisted of seven weld passes. Layer 3 consisted of four weld passes.

There are two major differences in terms of the laser parameters from the previous weld campaign:

(a) The power of the welding beam was reduced from 1000W to 700W for the entry pass of each layer (Pass 1 of Layer 1, Pass 1 of Layer 2, and Pass 1 of Layer 3).

(b) After welding each 3-layer clad, one additional autogenous pass (no filler wire) on each side of the weld toe regions of the first layer was performed. The center of the autogenous pass was aligned with the edge of the weld toe where the crack occurred in the last weld campaign (refer to **Figure 1**)

The purpose of these adjustments is to reduce and mitigate the formation of crack in the weld toe regions as observed in the previous weld campaign (M3LW-23OR0406015).

Note, abnormal welding parameters or conditions were accidentally used in some of the passes. They are summarized as follows:

(a) Sample ID 182C-4: insufficient shielding gas in weld passes 1 and 2 in Layer 1of clad L2 (low heat input with ABSI).

(b) Sample ID 182C-4: insufficient shielding gas in weld passes 8-10 in Layer 1of clad L3 (high heat input without ABSI)

(c) Sample ID 182D-3: insufficient shielding gas in weld pass 5 in Layer 1of clad L4 (high heat input with ABSI).

(d) Sample ID 182E-1: insufficient shielding gas from Pass 5/ Layer 2 to Pass1/layer 2 in clad L4 (high heat input with ABSI).

2.3 Weld microstructural characterization

A horizontal band saw was used in a hot cell to cut cross-weld samples from the welds made on irradiated coupons for weld quality, microstructure and property characterization. Samples for helium determination were removed by a low-speed diamond saw in a hot cell. Details of the cutting procedures can be found in the previous milestone report M3LW-23OR0406015 (Chen, et al. 2023). Optical imaging analysis was performed on the newly welded samples. Additionally, SEM analysis was conducted on one of the Alloy 182 samples welded in FY22 (M3LW-22OR0406013) to provide a statistical evaluation of the effects of the ABSI method.

3. RESULTS AND DISCUSSION

Figure 2(a-d) shows the cross-sections of welded 182C-4 sample (targeted 10 appm helium) containing four clads (L1-L4) welded with different conditions. **Figure 2 (a) and (c)** show the polished cross-sections, while (b) and (d) show the same cross-sections after etching. The etched cross-sectional view indicates the first pass (1) and the last pass (10) of the first clad layer, as well as the autogenous passes. No cracks are observed in clads L1 and L4 as shown in **Figure 2 (a) and (b)**. In contrast to previous results (M3LW-23OR0406015), which exhibited cracking at the weld toe of the first pass, the refined laser parameters used in the current welding campaign (reduced heat input for the first weld pass plus the additional low-heat autogenous passes on both weld toes) effectively mitigated this issue. However, as in **Figure 2 (c) and (d)**, a few cracks are still present. One crack is located between Passes 1 and 2 in L2, attributed to insufficient shielding gas protection, which led to increased laser heat absorption. For the same reason (insufficient shielding gas protection during welding Passes 8-10 in L3), a crack was also observed between Pass 10 and the adjacent autogenous pass in L3. The top views of the 182C-4 weld beads under these insufficient shielding gas conditions are shown in **Figure 3**, revealing a rough surface texture. Such roughness adversely affected the quality of subsequent fusion of the weld metal and contributed to lack of fusion (LOF) defects as indicated by a red box in **Figure 2 (c) and (d)**. This LOF defect is located in the deposited weld metal and has nothing to do with HeIC defect. It is noted that another crack is present on the top surface of L2. This crack is in the cladded material, not within the HAZ of the base metal, and is not attributed to HeIC either. The crack is believed to have been caused by excessive power of the auxiliary laser beam.

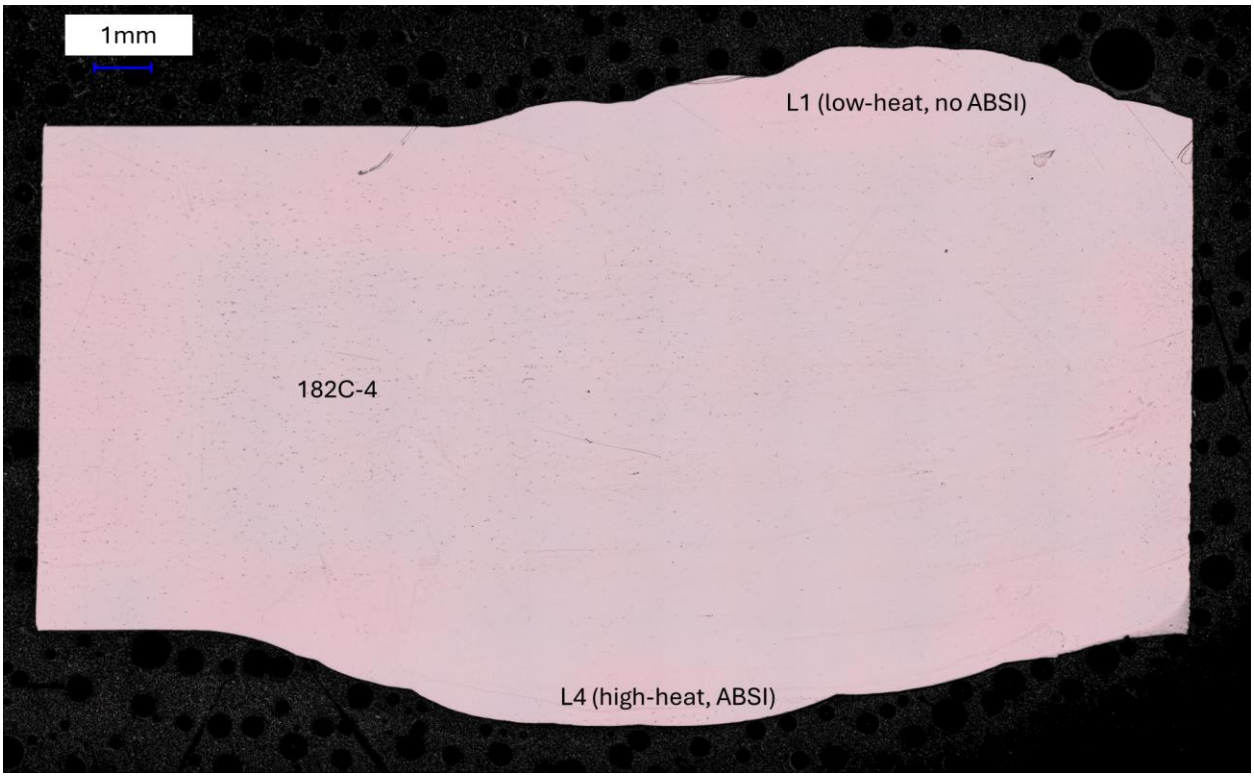

(a)

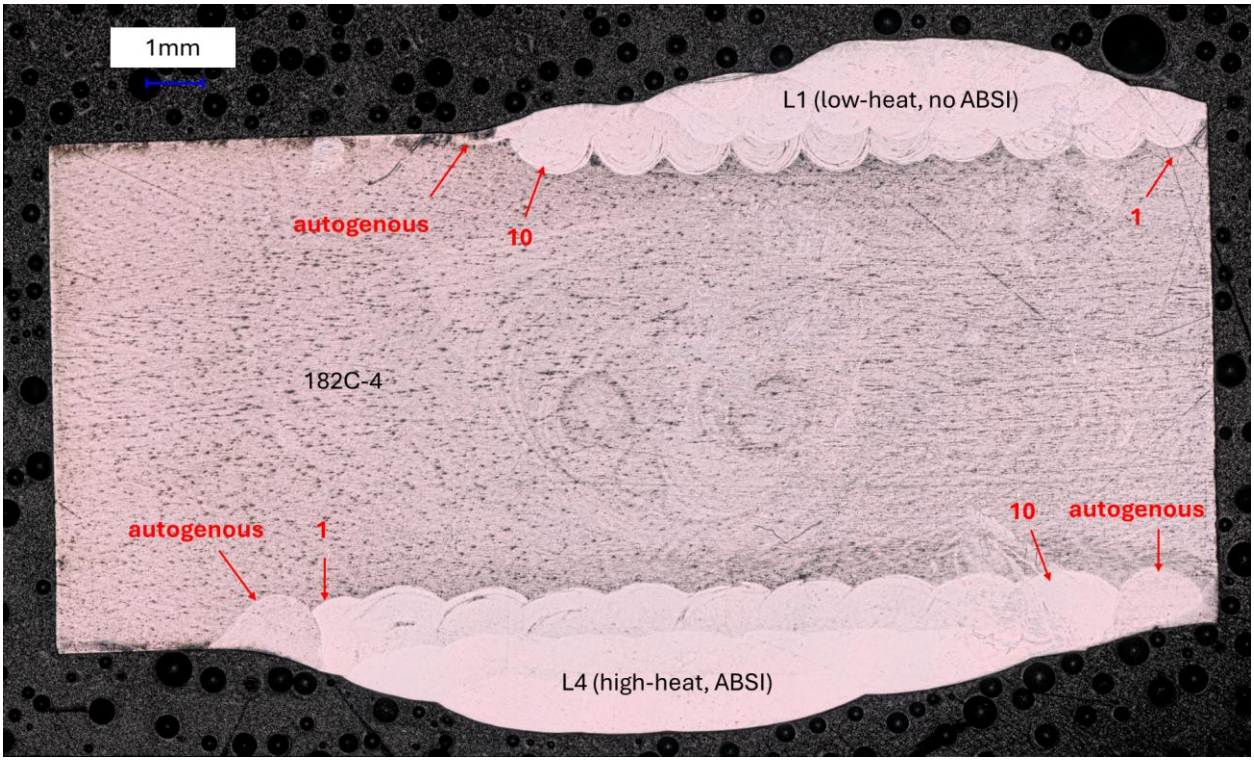
1mm
L1 (low-heat, no ABSI)
autogenous
10
1
182C-4
autogenous
1
10
autogenous
L4 (high-heat, ABSI)

(b)

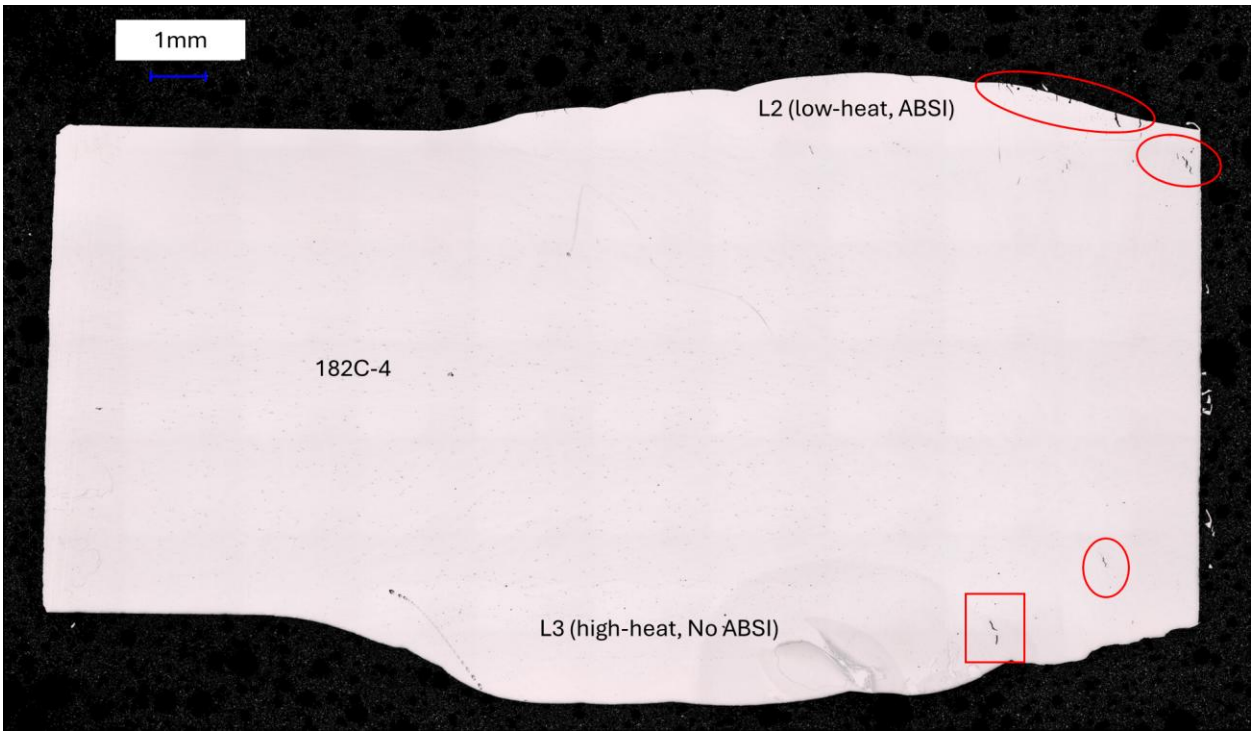
1mm
L2 (low-heat, ABSI)
182C-4
L3 (high-heat, No ABSI)

(c)

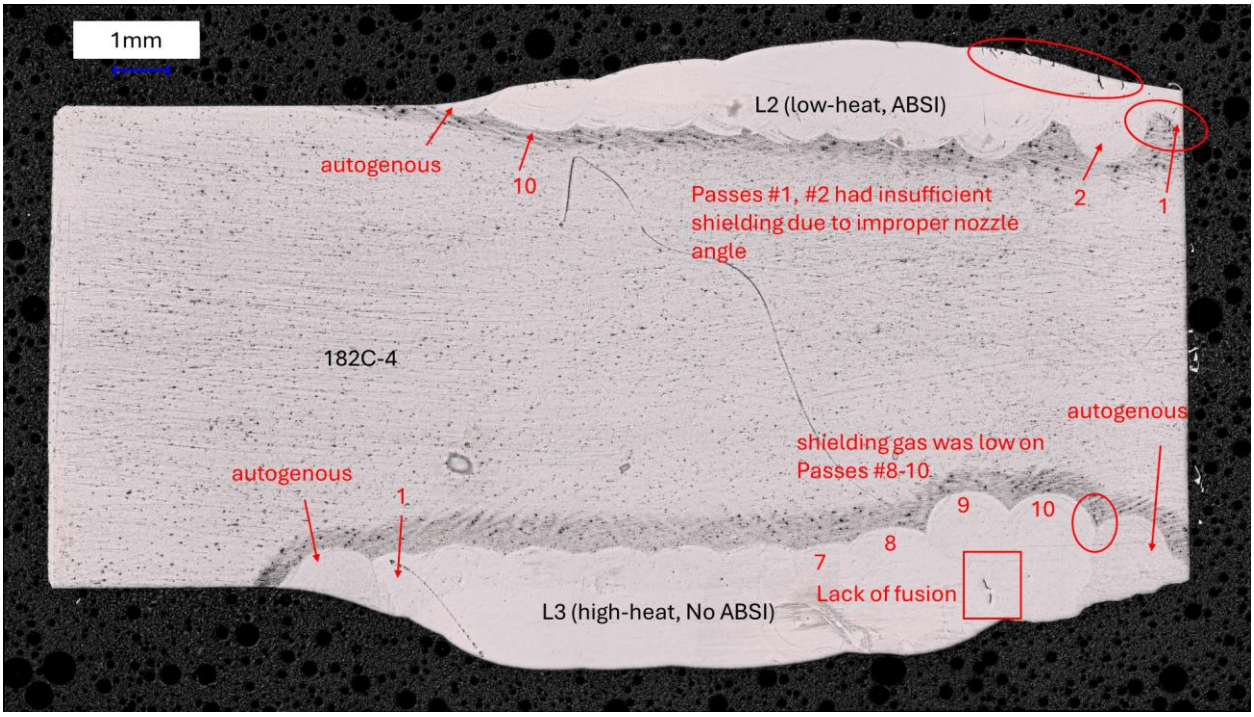

(d)

Figure 2 Cross-section views of 182C-4 welded coupon (targeted helium concentration 10 appm): polished (a) and etched (b) cross-section containing clad L1 (low heat input without ABSI) and clad L4 (high heat input with ABSI); polished (c) and etched (d) cross-section containing clad L2 (low heat input with ABSI) and clad L3 (high heat input without ABSI).

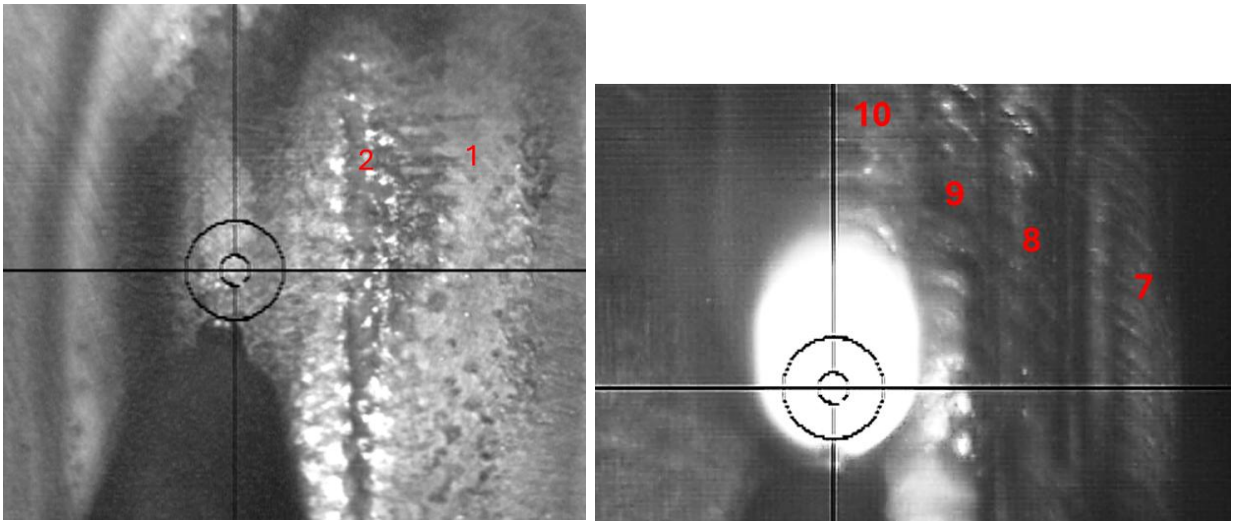

(a) (b)

Figure 3 Top views of the 182C-4 weld beads under insufficient shielding gas conditions: (a) Passes 1-2 in L2; (b) Passes 8-10 in L3.

Figure 4 and **Figure 5** present cross-sectional views of polished samples 182D-3 (nominally 20 appm targeted helium) and 182E-1 (nominally 30 appm targeted helium), respectively. Heat-affected zone (HAZ) cracks were observed along the fusion line boundary of the cladding in both samples. Overall, sample 182D-3 exhibits more cracks than 182E-1, despite having a lower nominal boron doping level. This discrepancy may be due to an actual transmuted helium concentration that differs from the nominal target. Further measurements are required to determine the actual helium content in the samples.

It is noted that shielding gas was insufficiently applied during welding Pass 5 of the first layer in L4 of sample 182D-3 (**Figure 4**a). This resulted in altered surface roughness, which affected several subsequent passes with increased heat input and penetration depth. These effects are also evident in the top-surface morphology of the weld (**Figure 6**a). Consequently, slightly larger cracks were observed in HAZ of the affected region in L4 of sample 182D-3, despite the application of ABSI, which was intended to reduce cracking (**Figure 4**a). For comparison, L3 of the same sample, where this issue was not present, shows slightly smaller cracks (**Figure 4**b).

A similar issue with shielding gas insufficiency occurred in L4 of sample 182E-1, as seen in the cross-sectional view(**Figure 5**a) and top view (**Figure 6**b). Although this occurred during welding of the second layer, the increased heat absorption led to a slight increase in HeIC tendency in HAZ.

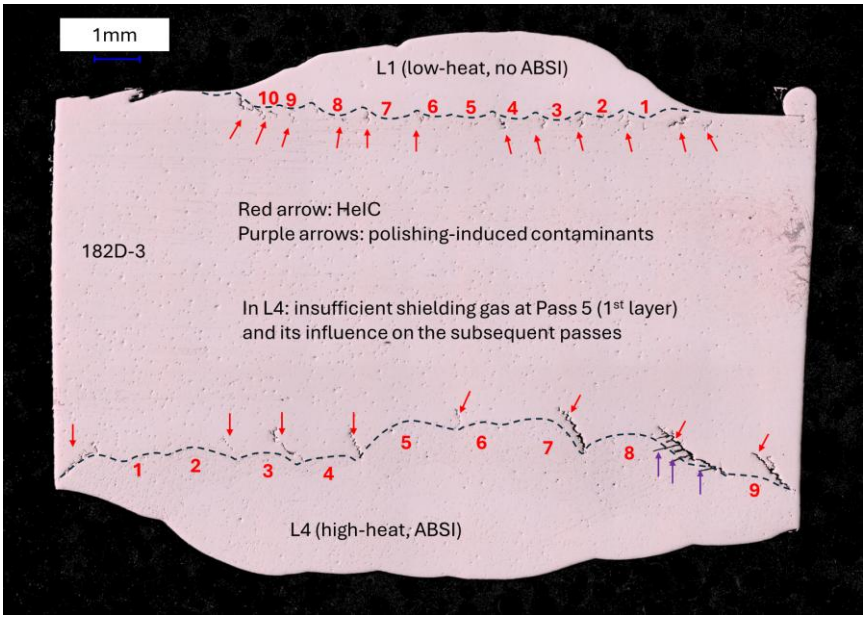

(a)

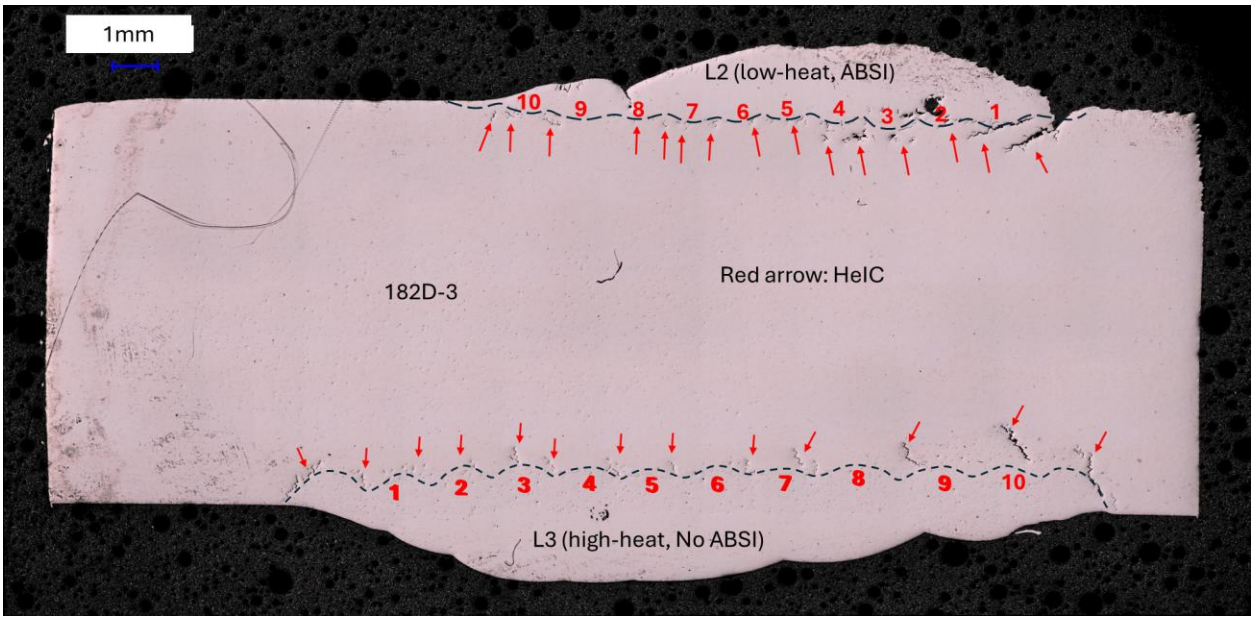

(b)

Figure 4 Cross-section views of polished 182D-3 coupon (targeted helium concentration 20 appm): (a) containing clad L1 (low heat input without ABSI) and clad L4 (high heat input with ABSI); (b) containing clad L2 (low heat input with ABSI) and clad L3 (high heat input without ABSI).

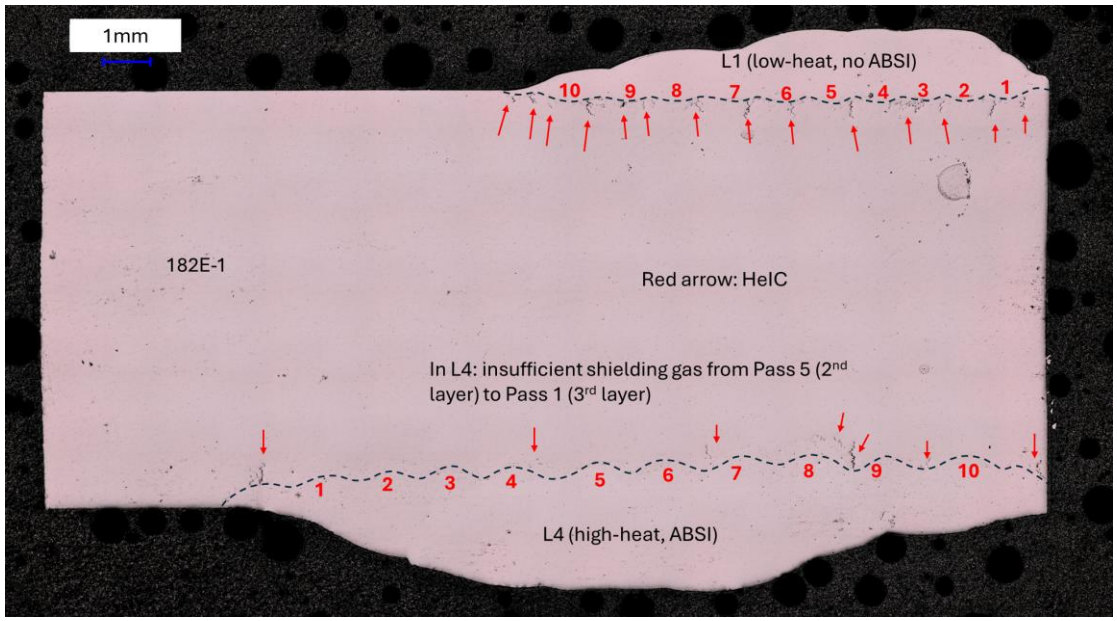

(a)

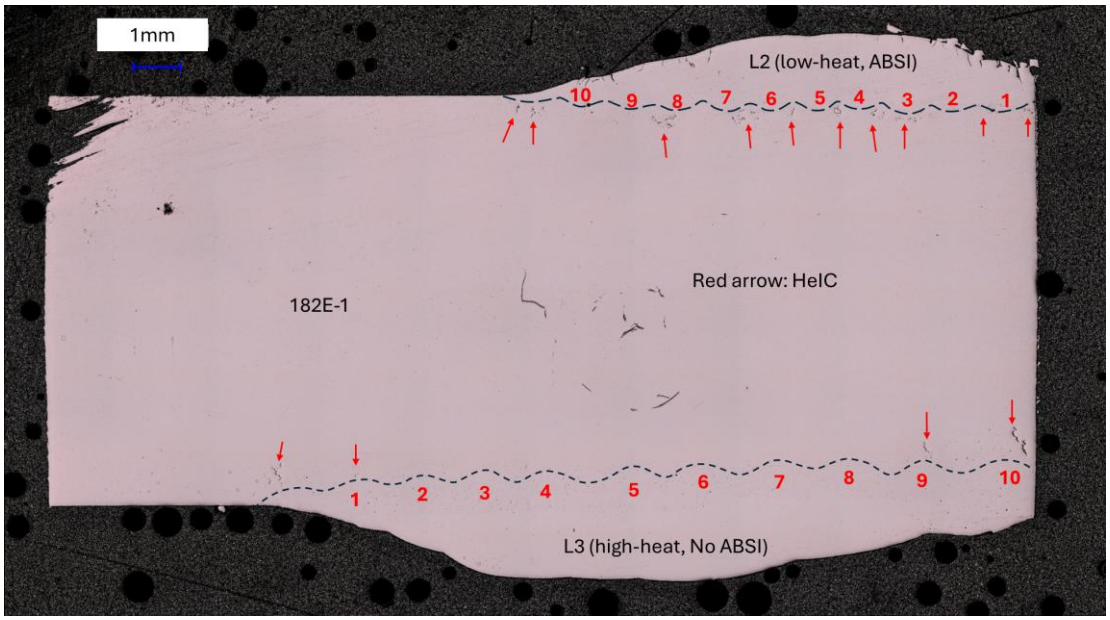

(b)

Figure 5 Cross-section views of polished 182E-1 coupon (targeted helium concentration 30 appm): (a) containing clad L1 (low heat input without ABSI) and clad L4 (high heat input with ABSI); (b) containing clad L2 (low heat input with ABSI) and clad L3 (high heat input without ABSI).

(a) 182D-3, L4 (high-heat, ABSI), 1st layer

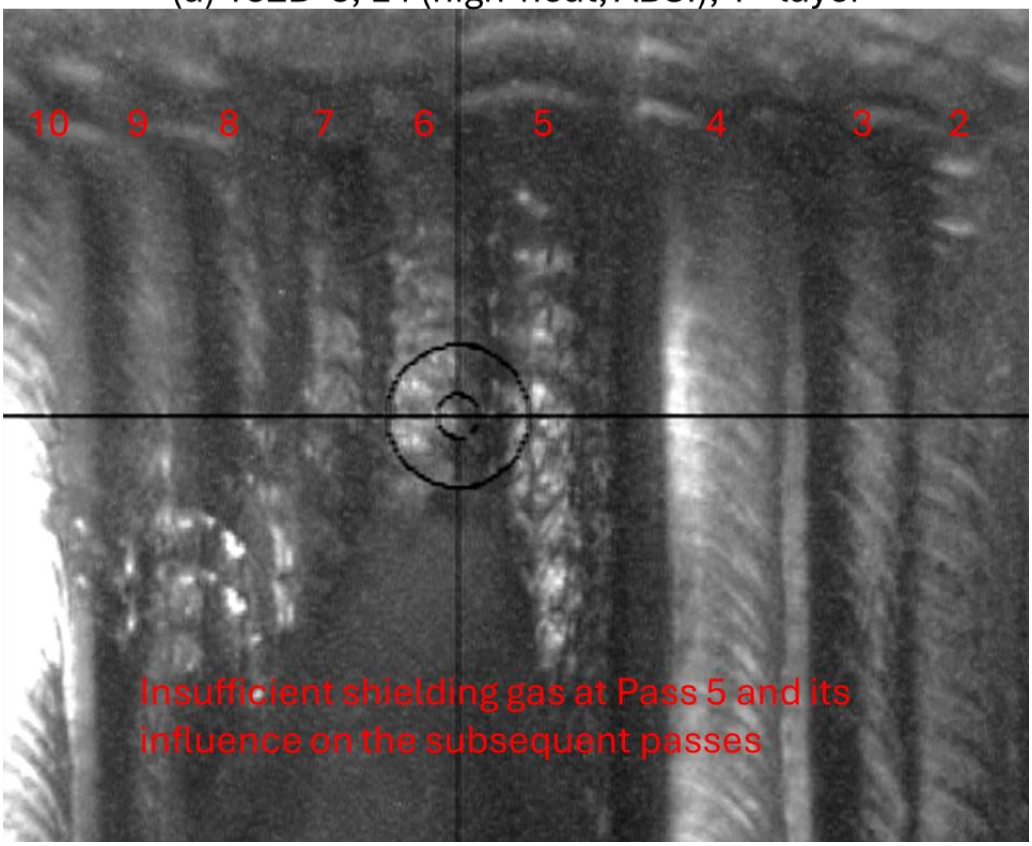

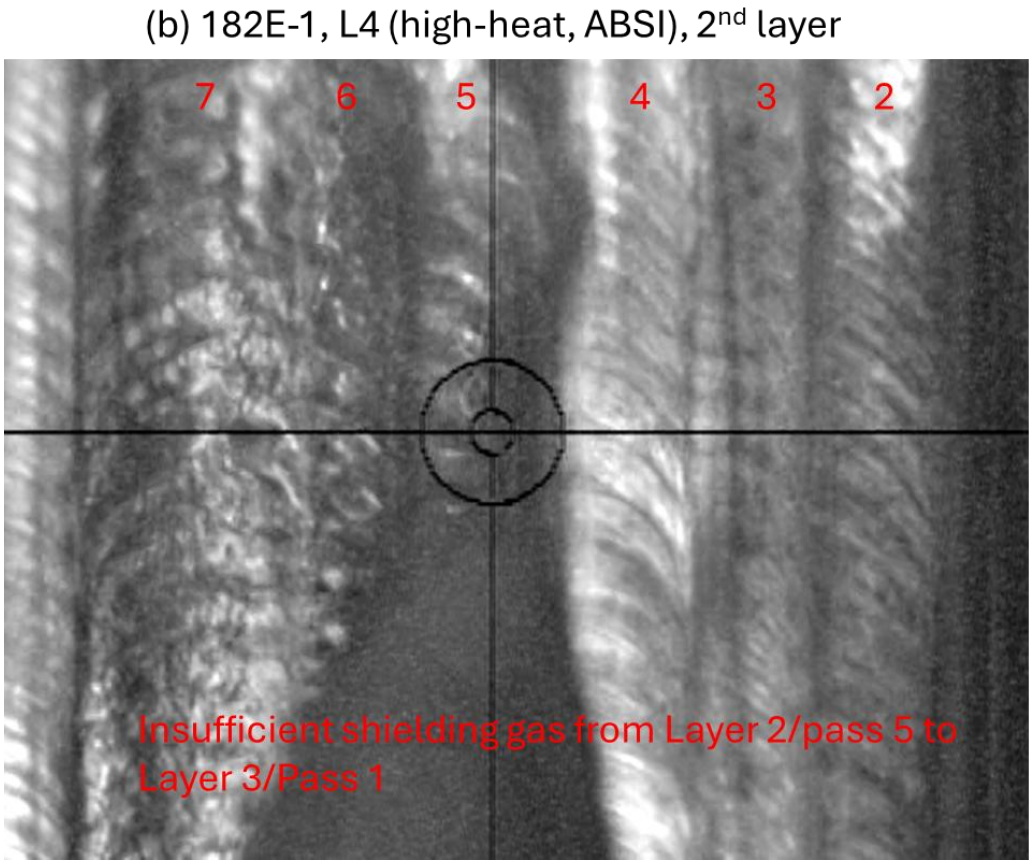

Figure 6 Top view of weld showing different surface morphology due to insufficient shielding gas protection: (a) 182D-3 and (b) 182E-1

To study the influence of ABSI on welding of Alloy 182, Coupons 182C-1-L1(low heat without ABSI) and 182C-1-L2 (low heat with ABSI), both welded in FY22 (M3LW-22OR0406013), were selected for further SEM analysis. In **Figure 7**a, sub-micron-sized pores or voids are visible within the FZ. Similar features have been reported in previous studies on welding irradiated stainless steels (M3LW-20OR0406016). These pores are not associated with HeIC but are instead attributed to helium entrapment during the solidification of the weld metal. In HAZ, microscopic cracks or pits (highlighted by arrows in the SEM image) were observed along some grain boundaries, consistent with observations from earlier welding trials on irradiated stainless steels. Similar submicron pores in FZ and signs of grain boundary degradation GBD in HAZ were also observed in the sample welded using ABSI technique as shown in **Figure 7**b. However, the extent of GBD appears to be reduced compared to the sample welded by the conventional method. This reduction can be attributed to the effect of the auxiliary beam in the ABSI setup, which introduces localized compressive thermal stresses around the weld zone. These compressive stresses help counteract the tensile stresses induced by solidification shrinkage, thereby suppressing grain boundary separation and limiting helium-induced damage during welding.

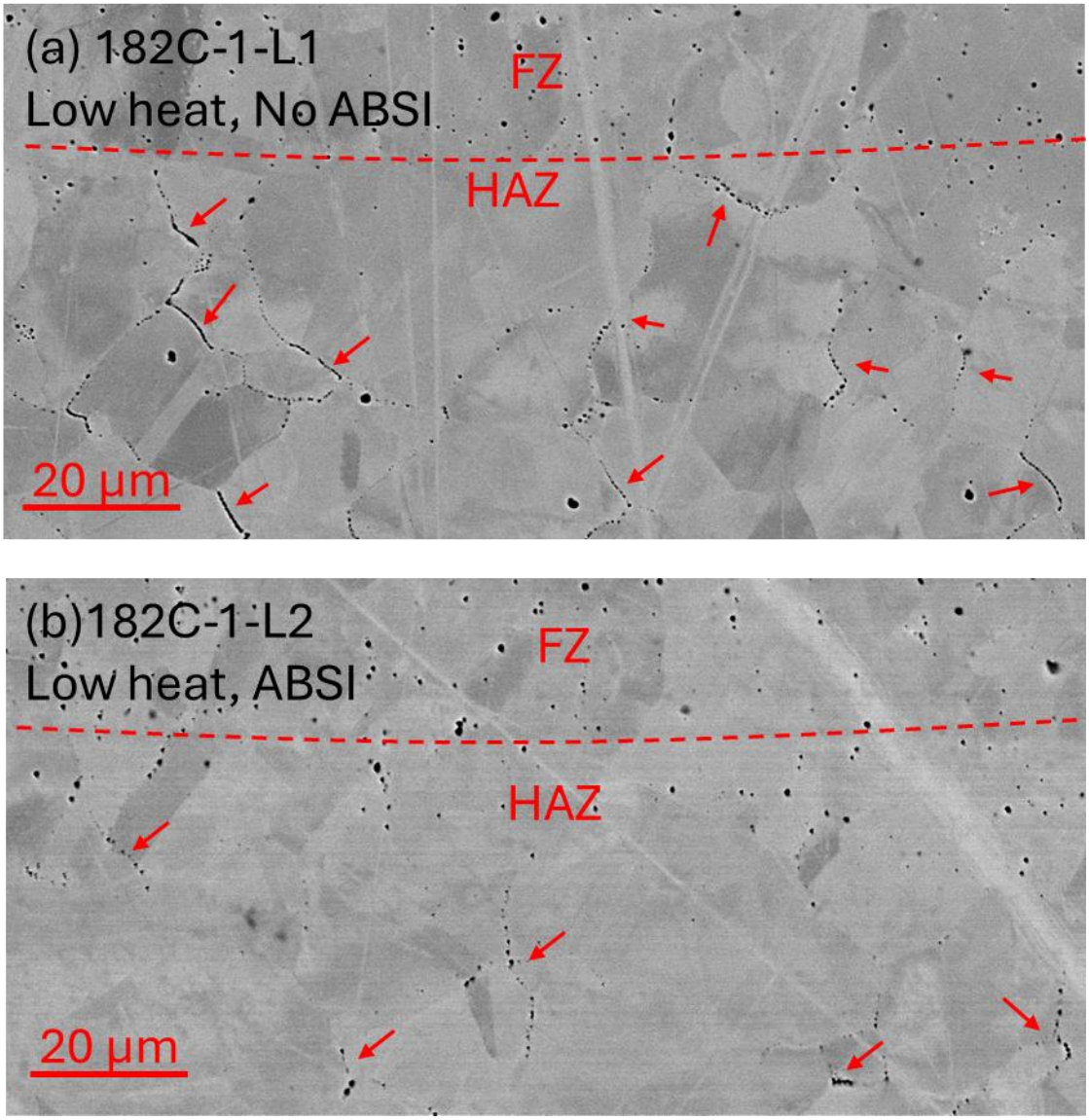

Figure 7 SEM images of (a) 182C-1-L1 and (b) 182C-1-L2 welded in FY22

A statistical comparison of microscale GBD was conducted by scanning along the entire fusion boundary using SEM. As shown in **Figure 8**, the overall extent of GBD was significantly lower in 182C-1-L2 welded using the ABSI technique compared to 182C-1-L1 welded with the conventional method. In the conventionally welded sample, approximately 1,230 GBDs were identified, with an average length of 10.2 µm and a maximum length of 53.7 µm. In contrast, the ABSI-welded sample exhibited only 339 GBDs, with a reduced average length of 7.1 µm and a maximum length of 38.4 µm. These results demonstrate the potential of the ABSI technique to mitigate GBD formation in helium-containing weldments.

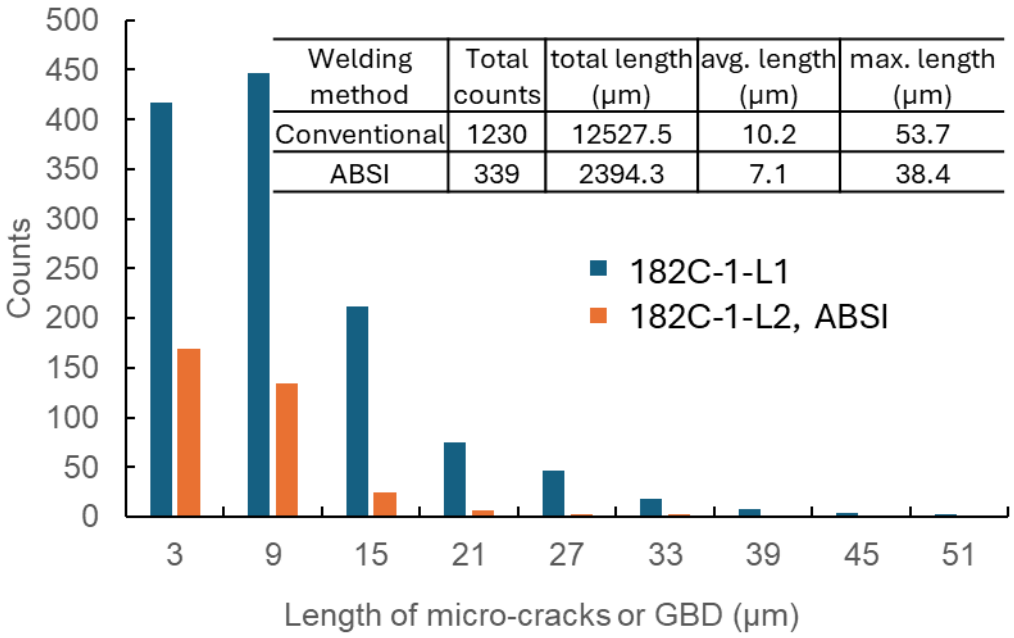

Figure 8 Statistical comparison of the microscopic GBD coupons 182C-1-L1 vs. 182C-1-L2

4. SUMMARY

This report describes the research activities conducted in FY 2025 on post-weld evaluation and characterization of the quality of welds made on irradiated Ni-base alloy 182 (with targeted helium from 10 to 30 appm) by refined laser welding conditions, with additional evaluation of welding techniques developed in prior years. The major findings include:

1. For samples with 10 appm targeted helium, refined laser process parameters (reduced power for the first pass plus low-heat autogenous passes on both sides of weld toe regions) show potential in mitigating HeIC at the weld toes, as observed in previous weld campaigns. However, insufficient shielding gas coverage can still lead to HeIC and lack of fusion defects.

2. For samples with targeted helium concentrations of 20 appm and above, HeIC was consistently observed along the fusion line in HAZ of each clad layer. These results indicate that the current laser process parameters do not provide sufficient mitigation of HeIC at these elevated helium levels, highlighting the need for further process optimization or alternative approaches for high-helium materials

3. To evaluate the influence of ABSI, SEM analysis was performed on two FY22 weld samples, one welded conventionally (182C-1-L1) and one using the ABSI technique (182C-1-L2). Both exhibited submicron-sized pores within the fusion zone, attributed to helium entrapment during solidification rather than HeIC. Microscopic GBD was observed in the HAZ of both samples. However, the extent of GBD was significantly reduced in the ABSI-welded sample.

5. REFERNECES

Asano, K., S. Nishimura, Y. Saito, H. Sakamoto, Y. Yamada, T. Kato and T. Hashimoto (1999). "Weldability of neutron irradiated austenitic stainless steels." Journal of Nuclear Materials **264**(1-2): 1-9.

EPRI (2015). BWRVIP-97, Revision 1: BWR Vessel and Internals Project, Guidelines for Performing Weld Repairs to Irradiated BWR Internals, EPRI.

Feng, Z., R. G. Miller, N. Cetiner, X. Hu, S. Clark, G. Frederick and B. Sutton (2017). Report Summarizing the Status of Second Round Irradiation Experiments and Assessment of Materials Available for Testing Advanced Welding (M3LW-17OR0406013). DOE Light Water Reactor Sustainability Program, Oak Ridge National Laboratory.

Feng, Z., R. G. Miller, J. Chen, M. Gussev, X. Hu, W. Tang, G. Frederick, J. Tatman and B. Sutton (2019). Recent Technological Advances in Welding Irradiated Helium Containing Austenitic Steel (M3LW-19OR0406015). DOE Light Water Reactor Sustainability Program, Oak Ridge National Laboratory.

Feng, Z., R. G. Miller, J. Chen, W. Tang, S. Clark, B. Gibson, M. Vance, G. Frederick, J. Tatman and B. Sutton (2017). Development of Welding Parameters for Irradiated Materials (M2LW-17OR0406014). DOE Light Water Reactor Sustainability Program, Oak Ridge National Laboratory.

Feng, Z., W. Tang, R. G. Miller, J. Chen, S. Clark, B. Gibson, G. Frederick, J. Tatman and B. Sutton (2018). Complete Report on Development of Weld Repair Technology (M2LW-18OR0406014). DOE Light Water Reactor Sustainability Program, Oak Ridge National Laboratory.

Feng, Z., W. Tang, R. G. Miller, J. Chen, M. Gussev, S. Clark, G. Frederick, J. Tatman and B. Sutton (2019). Develop Parameters and Characterize the Quality of Friction Stir and Laser Weld-Repaired, Irradiated Structural Materials Representative of Extended Reactor Service Life (M2LW-19OR0406014). DOE Light Water Reactor Sustainability Program, Oak Ridge National Laboratory.

Feng, Z. and G. M. Wilkowski (2002). Repair Welding of Irradiated Materials - Modeling of Helium Bubble Distributions for Determining Crack-Free Welding Procedures. 10th International Conference on Nuclear Engineering, ASME.

Feng, Z., K. Wolfe and E. Willis (2009). BWRVIP-228: BWR Vessel and Internals Project: A Computational Modeling Tool for Welding Repair of Irradiated Materials, EPRI.

JNES (2004). FY2003 Nuclear Power Plant Maintenance Improvement Technology (PMT), Japan Nuclear Energy Safety Organization.

JNES (2004). FY2003 Safe Maintenance/Repair Welding Techniques for Nuclear Plant Irradiated Materails (WIM), Japan Nuclear Energy Safety Organization.

Kanne Jr., W. R. (1988). "Remote Reactor Repair, GTA weld cracking caused by entrapped helium." Welding Journal(8): 33-39.

Lin, H. T., M. L. Grossbeck and B. A. Chin (1990). "Cavity Microstructure and Kinetics During Gas Tungsten Arc Welding of Helium-Containing Stainless Steel." Metallurgical Transactions A **21A**(9): 2585-2596.

Willis, E. (2006). BWRVIP-151: BWR Vessle and Internals Project, Technical Basis for Resision to BWRVIP-97 Welding Guidelines, EPRI.